Eur. Phys. J. Plus (2026) 141:359
https://doi.org/10.1140/epjp/s13360-026-07568-x

THE EUROPEAN PHYSICAL JOURNAL PLUS

Regular Article

Hawking radiation and gravitational lensing in quantum-modified black holes via the Gauss–Bonnet method

Erdem Sucu[a], **Izzet Sakallı**[b]

Physics Department, Eastern Mediterranean University, via Mersin 10, 99628 Famagusta Northern Cyprus, Türkiye

Received: 6 September 2025 / Accepted: 12 March 2026

Abstract This paper investigates the effects of quantum-modified effective metrics on black hole (BH) physics, with a focus on Hawking radiation and gravitational lensing phenomena. We employ the Gauss–Bonnet theorem to derive the Hawking temperature and deflection angles in spacetimes incorporating quantum corrections parameterized by ζ. Our analysis reveals how these corrections modify the Hawking temperature, creating distinct temperature profiles that deviate from classical predictions. We extend our study to examine gravitational lensing of both massless and massive particles using the optical and Jacobi metric formalisms, demonstrating significant modifications to deflection angles relative to general relativity. Furthermore, we analyze how surrounding media specifically cold non-magnetized plasmas and axion-plasmon fields-further alter light propagation, introducing frequency-dependent effects that could serve as observational signatures of quantum gravity. We also present orbital precession predictions for S-stars near Sgr A* as a test of the quantum-modified metric. Our results indicate that quantum-modified metrics can produce measurable deviations in lensing observables, which may serve as targets for future precision tests of quantum gravity.

1 Introduction

The incorporation of quantum gravity corrections into BH physics has fundamentally transformed our understanding of these extreme gravitational systems. Classical general relativity, while remarkably successful in many regimes, fails to capture the quantum fluctuations that become significant near BH singularities and event horizons. Effective metrics have emerged as crucial constructs that bridge classical and quantum descriptions of gravity while preserving covariance. Pioneering work in loop quantum gravity by Bojowald [1] and Ashtekar [2] predicted substantial deviations from classical spacetime near the Planck scale, while Zhang et al. [3] developed effective metrics that introduce the parameter ζ to quantify these quantum modifications.

The thermodynamic properties of BHs represent one of the most notable connections between quantum mechanics and gravity. Since Hawking's discovery of BH radiation [4], researchers have sought methods to calculate BH temperature. The Gauss–Bonnet (GB) theorem has emerged as a powerful topological approach, connecting the Euler characteristic of a two-dimensional Riemannian manifold to its Gaussian curvature (GC). Applied to quantum-modified spacetimes, this method reveals how quantum effects alter temperature profiles, with possible relevance to the information paradox [5].

Gravitational lensing [6–18] provides a critical observational window into spacetime geometry. Building on Einstein's prediction of light deflection [19, 20], Gibbons and Werner [21] pioneered the application of the GB theorem to calculate deflection angles by integrating GC over appropriate domains. This technique has been extended to modified gravity theories [22–24], revealing how quantum corrections influence light propagation near compact objects. For massive particles, the Jacobi metric formalism recasts particle dynamics as geodesic motion in an effective spatial geometry [25–27], allowing unified treatment of gravitational lensing for both massless and massive test bodies. These approaches are particularly relevant for understanding dark matter dynamics and testing modified gravity theories [28, 29]. Astrophysical environments further complicate this picture. Cold non-magnetized plasmas introduce frequency-dependent refraction [30, 31], creating chromatic effects in gravitational lensing that become significant in environments with high electron density. The possible existence of axion fields, hypothetical particles proposed as dark matter candidates, adds another layer of complexity through axion–photon coupling in magnetic fields [32, 33], producing distinctive lensing signatures that could serve as observational probes for axion dark matter. Recent astronomical observations, together with upcoming facilities such as SKA [34] and LISA [35], promise increasingly precise constraints on deviations from general relativity in strong gravitational fields.

[a] e-mail: erdemsc07@gmail.com
[b] e-mail: izzet.sakalli@emu.edu.tr (corresponding author)

Published online: 31 March 2026

In addition, we incorporate quantum corrections via the Generalized Uncertainty Principle (GUP) [36–49], which introduces a fundamental minimal length at the Planck scale. The GUP framework extends BH thermodynamics by providing higher-order corrections to the Hawking temperature, potentially stabilizing evaporation and suggesting the existence of BH remnants [50–52]. This extension allows us to probe how quantum gravity effects manifest not only through effective metric modifications but also through modified uncertainty relations, offering complementary views on BH evaporation dynamics [53–55].

Our work explores how quantum-induced modifications to spacetime geometry, parameterized by ζ, affect BH observables across multiple domains: Hawking temperature profiles, gravitational lensing of both massless and massive particles, and light propagation through plasma and axion-plasmon media. By establishing quantitative relationships between quantum parameters and observable effects, we bridge theoretical developments with potential astronomical observations while examining connections between effective metrics and dark matter-like effects.

Recently, an alternative treatment of light and particle deflection in covariant quantum gravity frameworks was developed in Ref. [56], where the authors employed the GB theorem to analyze both massless and massive particle trajectories in effective geometries with quantum corrections of the form $f(r) = 1-2M/r \pm 2\zeta M^2/r^2$. While their approach uses effective theory modifications where quantum corrections enter through modified constraint structures, our formulation relies on the covariant model introduced in Ref. [57] that preserves the geometric structure of spacetime through quantum corrections arising from modified Hamiltonian constraints while maintaining 4D diffeomorphism invariance. The quantum parameter ζ in our work encodes quantum gravity effects through modified constraint algebra, differing fundamentally from the coupling parameter definition used in Ref. [56]. Despite both works utilizing the GB method as a topological tool to extract deflection angles, the distinct theoretical frameworks, quantum correction structures, and resulting expressions reflect different mathematical structures of quantum gravity approaches. To elucidate these differences, we provide a dedicated comparative analysis in Section 4.1, where we clarify the source of these discrepancies and highlight the consistency of our results within the framework adopted here.

The paper proceeds as follows: Section 2 reviews effective metrics in curved spacetime. Section 3 applies the GB theorem to calculate Hawking temperature and includes GUP-corrected modifications. Section 4 investigates gravitational lensing in effective spacetimes and analyzes photon sphere stability. Section 5 extends the analysis to massive particles using the Jacobi metric formalism. Sections 6 and 7 incorporate plasma effects and axion-plasmon media influences, respectively. Section 8 presents orbital precession predictions for S-stars near Sgr A*. Section 9 summarizes our findings and discusses their implications for observational astronomy and fundamental physics.

2 Review of effective metrics in curved spacetime

Given the effective Hamiltonian constraints derived from loop quantum gravity, the associated spacetime metric can be expressed in a modified form incorporating quantum effects that preserve general covariance. Our approach employs quantum corrections arising from effective Hamiltonian constraints while maintaining 4D diffeomorphism invariance, where the quantum parameter ζ encodes quantum gravity effects through modified constraint algebra. The general form of the effective line element is given by [57]:

$$ds^2 = -N^2dt^2 + \frac{(E^2)^2}{\mu E^1}(dr + N^r dt)^2 + E^1 d\Omega^2, \tag{1}$$

where $d\Omega^2 = d\theta^2 + \sin^2\theta d\phi^2$ represents the standard metric on S^2, and the function μ encodes quantum corrections. The primary requirement for covariance is that this metric remains invariant under coordinate transformations induced by the modified Hamiltonian constraints.

To ensure consistency with the quantum-modified Hamiltonian dynamics, the modified structure function S defined as $S = \mu E^1/(E^2)^2$ plays a crucial role in maintaining the closure of the constraint algebra [57]:

$$\{H_r[N_1^r], H_r[N_2^r]\} = H_r[N_1^r\partial_r N_2^r - N_2^r\partial_r N_1^r], \tag{2}$$

$$\{H_r[N^r], H_{\text{eff}}[N]\} = H_{\text{eff}}[N^r\partial_r N], \tag{3}$$

$$\{H_{\text{eff}}[N_1], H_{\text{eff}}[N_2]\} = H_r[S(N_1\partial_r N_2 - N_2\partial_r N_1)]. \tag{4}$$

Here, the diffeomorphism generators are defined locally as $\xi^\mu = (N_1, E_1, \ldots)$, acting on the radial coordinate r. The associated local diffeomorphism algebra satisfies the standard closure relations under Lie brackets. By solving these conditions, the first effective metric, which is the focus of our analysis, takes the form:

$$ds^2_{(1)} = -f_1(r)dt^2 + f_1(r)^{-1}dr^2 + r^2 d\Omega^2, \tag{5}$$

where the function $f_1(r)$ is defined as [57]:

$$f_1(r) = 1 - \frac{2M}{r} + \frac{\zeta^2}{r^2}\left(1 - \frac{2M}{r}\right)^2. \tag{6}$$

The absence of linear terms in ζ reflects the parity symmetry $\zeta \to -\zeta$ of the underlying effective Hamiltonian, where quantum corrections enter through quadratic expectation values of the holonomy-like connection variables. Consequently, only even powers of ζ appear at the level of the metric, with higher-order contributions $\mathcal{O}(\zeta^4)$ suppressed by additional factors of $(M/r)^2$ and neglected at leading order. We note that higher powers of ζ naturally emerge in derived quantities such as curvature invariants, deflection angles, and thermodynamic observables, due to nonlinear combinations of $f_1(r)$ and its derivatives; however, these all originate from the single ζ^2 factor in the metric. This metric exhibits a double-horizon structure similar to the Reissner–Nordström solution, where the outer and inner horizons are located at $r_+ = 2M$ and $r_- = \zeta^2/\beta - \beta/3$, with $\beta^3 = 3\zeta^2(\sqrt{81M^2 + 3\zeta^2} - 9M)$. The parameter ζ quantifies the strength of quantum corrections to the classical Schwarzschild geometry and plays a central role in determining the physical properties of these quantum-modified BHs (QMBHs). Physically, the parameter ζ arises from the modified Hamiltonian constraint algebra in loop quantum gravity [57]. It encodes the magnitude of the quantum deformation of spacetime curvature and has the same dimensionality as the BH mass in geometrized units. For astrophysical BHs one expects $\zeta/M \ll 1$, while the larger ζ values used in our figures serve only to illustrate qualitative trends. Thus, ζ effectively measures the strength of near-horizon quantum corrections, disappearing smoothly in the classical limit.

We note that the framework of Ref. [57] also admits a second effective metric solution $ds^2_{(2)}$, incorporating a modification factor μ_2 that regularizes the interior geometry and produces a bounce-like transition relevant for interior dynamics. Since the present study focuses on exterior observables—Hawking radiation, lensing, and orbital precession—we employ exclusively the first metric $ds^2_{(1)}$ throughout. The modified metric considered here effectively encodes quantum corrections through the parameter ζ, without the need to introduce an auxiliary or secondary metric structure.

Furthermore, an analysis of the effective energy-momentum tensor $T^q_{\rho\sigma} = G_{\rho\sigma}/(8\pi)$ reveals a quantum-induced energy density:

$$\rho_q = \frac{\zeta^2(r-6M)(r-2M)}{8\pi r^6}, \tag{7}$$

Although Eq. (7) allows regions where $\rho_q < 0$ (for $2M < r < 6M$), this does not signal an instability. Such negative energy domains arise from quantum vacuum polarization, analogous to Casimir-type effects in semiclassical gravity. Their magnitude scales as ζ^2 and therefore remains extremely small for $\zeta/M \ll 1$, ensuring that the exterior spacetime is stable and physically meaningful, suggesting a potential link between quantum modifications and dark matter-like effects.

Throughout the subsequent sections, we focus our analysis on the first effective metric $ds^2_{(1)}$, investigating its Hawking temperature through the GB theorem and its gravitational lensing effects in various environments. For clarity, all analytical derivations and numerical results presented in the following sections are obtained exclusively using the first effective metric, characterized by the function $f_1(r)$.

3 Calculation of Hawking temperature via GB theorem

The topological method used to determine the Hawking temperature was developed based on the two-dimensional Euler characteristic and the GB theorem [58]. To understand the basic structure of this method, let us first consider the four-dimensional, spherically symmetric, and stationary BH metric (5) with $f_1(r)$. This metric can be reduced to two-dimensional Euclidean Schwarzschild coordinates by choosing the Wick transformation ($\tau = it$) and $\theta = \frac{\pi}{2}$:

$$ds^2 = f_1(r)d\tau^2 + \frac{1}{f_1(r)}dr^2. \tag{8}$$

The Ricci scalar curvature of this metric can be calculated as follows:

$$R = -\frac{d^2}{dr^2} f_1(r). \tag{9}$$

The general formula used to obtain the Hawking temperature by the topological method is as follows:

$$T_H = \frac{\hbar c}{4\pi \chi k_B} \sum_{j \le \chi} \int_{r_{h_j}} \sqrt{g} R dr. \tag{10}$$

Here $\hbar$ is the Planck constant, c is the speed of light and k_B is the Boltzmann constant. In addition, R is a function of spatial coordinates r only, and g is the Euclidean metric determinant. r_{h_j} represents the Killing horizon, while χ is the Euler characteristic of Euclidean geometry. The expression $\sum_{j \le \chi}$ shows the sum over all Killing horizons.

From this point on, formulas and metrics will be simplified by taking all physical constants as units. Applying this method to our quantum-modified metric with the function $f_1(r)$ as defined in Section 2, we obtain the Hawking temperature for the QMBH:

$$T_H = \left.\frac{f_1'(r)}{4\pi}\right|_{r=r_h} = \frac{2M}{4\pi r_h^2} - \frac{2\zeta^2}{4\pi r_h^3} + \frac{12M\zeta^2}{4\pi r_h^4} - \frac{16M^2\zeta^2}{4\pi r_h^5} \tag{11}$$

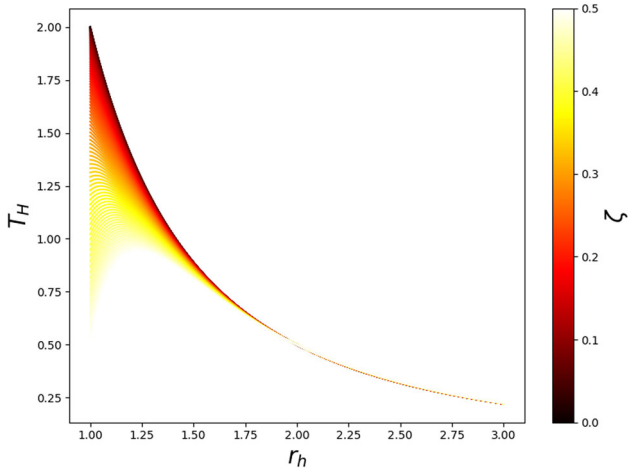

Fig. 1 Temperature T_H as a function of r_h for varying ζ, with fixed parameter $M = 1$. The values of ζ used in the figures are chosen for illustrative purposes. For astrophysical BHs, $\zeta/M \ll 1$ and the corrections are perturbatively small

Figure 1 shows the variation of Hawking temperature (T_H) with event horizon radius (r_h) for different ζ values ($\zeta = 0.01, 0.02, 0.03$). For small r_h values, the temperature increases rapidly, but after reaching a certain maximum point, it exhibits an asymptotic behavior by decreasing. For smaller ζ values, the temperature is initially higher and shows a monotonic decrease, while for large ζ values, a distinct maximum point appears. Especially for $\zeta = 0.03$, the maximum temperature is evident, after which the temperature starts to decrease. This shows that ζ changes the location and value of the maximum temperature point. For large ζ values, the temperature starts lower at the small radii of the event horizon and then increases. These modified thermal properties may influence evaporation dynamics at late stages and could be relevant for discussions of information retention in quantum-corrected BH models [59].

We emphasize that the Hawking temperature obtained here is not conceptually new, but is rederived using the GB's topological method in the context of the quantum-modified effective metric under consideration. This approach allows a geometric consistency check and provides a unified framework compatible with subsequent lensing analyses. An important feature revealed by Fig. 1 is the existence of a zero-temperature configuration at finite horizon radius for nonzero ζ, signaling the formation of a BH remnant. To analyze this, we first note that the outer horizon satisfies $r_+ = 2M$ regardless of ζ. Substituting $r_h = 2M$ into Eq. (11) yields $T_H = 1/(8\pi M)$, with all ζ-dependent corrections cancelling identically. This confirms that the Hawking temperature at the outer horizon remains purely Schwarzschild. Since the outer horizon is fixed at $r_+ = 2M$ independent of ζ, expressing T_H solely in terms of M via $M = r_h/2$ would suppress all quantum corrections and reduce the result to the standard Schwarzschild form, obscuring the effects under study. The nontrivial quantum-modified thermal behavior, including the remnant feature, is associated with the inner horizon r_-, whose location depends explicitly on ζ. This is why Eq. (11) retains both M and r_h in its general form, correctly capturing the temperature at both horizons. The remnant condition $T_H = 0$, equivalently $f_1'(r_h \equiv r_{\rm rem}) = 0$, leads to the cubic equation:

$$M r_{\rm rem}^3 - \zeta^2 r_{\rm rem}^2 + 6M\zeta^2 r_{\rm rem} - 8M^2\zeta^2 = 0. \tag{12}$$

For small ζ/M, the critical remnant radius behaves as $r_{\rm rem} \approx \zeta^2/M + \mathcal{O}(\zeta^4/M^3)$, vanishing smoothly in the classical limit $\zeta \to 0$. This zero-temperature state implies that the quantum-modified BH ceases to emit Hawking radiation at a finite mass, leaving behind a stable remnant. Such remnant configurations are absent in the classical Schwarzschild geometry and may carry implications for the information paradox and the existence of Planck scale relics [60, 61].

3.1 GUP-corrected Hawking temperature

The semiclassical Hawking temperature derived above relies on a fixed background geometry with quantum corrections encoded in the metric parameter ζ. However, an independent class of quantum modifications arises at the kinematic level from the GUP, which introduces a fundamental minimal length associated with the Planck scale. While the ζ-dependent corrections modify the spacetime geometry itself, GUP-induced corrections act at the level of local kinematics by modifying uncertainty relations and particle energies. To leading order, these effects can be treated as independent, since they originate from distinct aspects of quantum gravity. Examining both within the same thermodynamic section allows a direct comparison of their relative impact on the Hawking temperature.

BH thermodynamics is typically derived in a semiclassical regime, where the gravitational field is treated classically while quantum effects are restricted to matter fields. Although this approximation yields the celebrated results of Hawking radiation and Bekenstein entropy, it is expected to break down in the vicinity of the Planck scale, where full quantum gravity corrections cannot be neglected [62, 63]. At such microscopic scales, the nature of spacetime is governed by strong fluctuations, and the very concepts of

distance and time intervals lose their classical meaning. This motivates the inclusion of quantum modifications to the thermodynamic framework, one of the most widely studied being the GUP [64, 65].

The GUP extends the Heisenberg uncertainty principle by incorporating a fundamental minimal length, l_p, commonly associated with the Planck length

$$l_p = \sqrt{\frac{\hbar G}{c^3}} \sim 10^{-35}\,\mathrm{m}, \tag{13}$$

which is expected to play the role of a natural cutoff for spacetime resolution. In its quadratic form, the GUP reads

$$\Delta x\,\Delta p \geq \hbar\left(1+\lambda^2\frac{l_p^2}{\hbar^2}\Delta p^2\right), \tag{14}$$

where λ is a dimensionless constant encoding the strength of the quantum gravity effects.

Solving Eq. (14) for the momentum uncertainty gives

$$\Delta p \geq \frac{\Delta x}{2\lambda^2 l_p^2}\left(\sqrt{1+\frac{4\lambda^2 l_p^2}{(\Delta x)^2}}-1\right). \tag{15}$$

For BHs with horizon radius much larger than l_p, one may expand the square root in Eq. (15) as a series:

$$\Delta p \simeq \frac{1}{\Delta x}\left(1+\frac{\lambda^2 l_p^2}{(\Delta x)^2}-\frac{\lambda^4 l_p^4}{2(\Delta x)^4}+\mathcal{O}\left(\frac{l_p^6}{(\Delta x)^6}\right)\right). \tag{16}$$

When the uncertainty relation is saturated, $\Delta x\Delta p \simeq 1$, the particle energy near the horizon acquires a correction:

$$E_{GUP} \simeq \frac{1}{\Delta x}\left(1+\frac{\lambda^2 l_p^2}{(\Delta x)^2}-\frac{\lambda^4 l_p^4}{2(\Delta x)^4}\right). \tag{17}$$

Identifying $\Delta x \approx 2r_h$, as suggested by near-horizon tunneling analyses [63], we obtain

$$E_{GUP} \simeq \frac{1}{2r_h}\left(1+\frac{\lambda^2 l_p^2}{4r_h^2}-\frac{\lambda^4 l_p^4}{32r_h^4}\right). \tag{18}$$

The semiclassical tunneling probability of an emitted particle with energy E is given by

$$\Gamma_0 \sim \exp\left(-\frac{4\pi E}{f_1'(r_h)}\right), \tag{19}$$

where $f_1'(r_h)$ is the derivative of the metric function evaluated at the horizon. Incorporating the corrected energy E_{GUP} from Eq. (18) modifies the tunneling rate to

$$\Gamma \sim \exp\left(-\frac{4\pi E_{GUP}}{f_1'(r_h)}\right). \tag{20}$$

Comparing Eq. (20) with the Boltzmann factor $\exp(-E/T)$ allows us to identify the GUP-corrected Hawking temperature:

$$T_{GUP} \simeq T_H\left(1+\frac{\lambda^2 l_p^2}{4r_h^2}-\frac{\lambda^4 l_p^4}{32r_h^4}\right), \tag{21}$$

where T_H is the uncorrected Hawking temperature given in Eq. (11). Equation (21) demonstrates that the inclusion of GUP effects increases the BH temperature relative to the semiclassical value, with the correction terms becoming increasingly dominant as the horizon radius approaches the Planck scale. The higher-order terms ($\sim r_h^{-4}$ and beyond) indicate possible stabilization mechanisms, suggesting the existence of BH remnants that could halt the complete evaporation process. It is noteworthy that the remnant formation mechanism identified here through GUP corrections complements the metric-level remnant condition derived in Eq. (12): both the geometric (ζ) and kinematic (λ) quantum corrections independently predict the cessation of Hawking evaporation at finite mass, reinforcing the consistency of the remnant scenario across different quantum gravity frameworks.

In summary, the quantum-modified BH under consideration receives thermodynamic corrections from two independent sources: (i) the metric-level parameter ζ, which modifies the spacetime geometry and alters the surface gravity, and (ii) the GUP parameter λ, which modifies the near-horizon particle kinematics. These corrections enter multiplicatively in Eq. (21), with each encoding a distinct physical mechanism. A natural extension of the present work would be to derive the Hawking spectrum through the Bogoliubov coefficient method and the Hamilton–Jacobi tunneling formalism with residue integration [66, 67], which would provide a complete thermodynamic characterization of the QMBH, including greybody factors and entropy corrections. A fully unified treatment incorporating both contributions simultaneously is left for future work.

4 Gravitational lensing in effective spacetimes

In this section, we provide an overview of the GB theorem and employ it to determine the small deflection angle for the effective BH. We stress that although the GB method has been applied to quantum-corrected metrics in previous studies (e.g., Ref. [56]), the specific metric function adopted here, Eq. (6), differs structurally from those considered earlier. In particular, our metric involves $\zeta^2(1-2M/r)^2/r^2$ rather than a linear $\zeta M^2/r^2$ correction, and the resulting deflection angles are therefore new and cannot be obtained from existing results by simple reparametrization. We begin by considering the null geodesics that satisfy $ds^2 = 0$. Rearranging the metric yields the following

$$dt^2 = \gamma_{ij}dx^i dx^j = \frac{1}{f_1^2(r)}dr^2 + \frac{r^2}{f_1(r)}d\Omega^2. \tag{22}$$

where i and j take values from 1 to 3, and γ_{ij} denotes the optical metric. Applying the coordinate transformation $dr^* = \frac{1}{A}dr$, the metric can be rewritten as:

$$dt^2 = dr^{*2} + \tilde{f_1}^2(r^*)d\phi^2, \tag{23}$$

where $\tilde{f_1}(r^*) \equiv \sqrt{\frac{r^2}{f_1(r)}}$ and $\theta = \frac{\pi}{2}$.

To utilize the GB theorem, the GC must be computed. The curvature expression is given by:

$$\mathcal{K} = \frac{R_{r\phi r\phi}}{\gamma} = \frac{1}{\sqrt{\gamma}}\left[\frac{\partial}{\partial\phi}\left(\frac{\sqrt{\gamma}}{\gamma_{rr}}\Gamma^{\phi}_{rr}\right) - \frac{\partial}{\partial r}\left(\frac{\sqrt{\gamma}}{\gamma_{rr}}\Gamma^{\phi}_{r\phi}\right)\right]. \tag{24}$$

Thus, for our quantum-modified effective metric, we find:

$$\mathcal{K} = \frac{2M}{r^3} + \left(\frac{3}{r^4} - \frac{30M}{r^5}\right)\zeta^2. \tag{25}$$

where γ represents the determinant of γ_{ij}, and R is the Ricci scalar.

Consider a domain D, a compact, oriented, and nonsingular two-dimensional Riemannian surface with Euler characteristic $\chi(D)$ and GC $\mathcal{K}$. The boundary consists of a smooth piecewise curve with geodesic curvature κ. The GB theorem relates the deflection angle to curvature via:

$$\int\int_D \mathcal{K}dS + \oint_{\partial D}\kappa dt + \sum_{i=1}\beta_i = 2\pi\chi(D). \tag{26}$$

where dS is the surface element, $\kappa = |\nabla_{\dot{C}}\dot{C}|$ is the geodesic curvature, and β_i represents the exterior angles. Choosing a domain $\tilde{D}$, enclosed by a geodesic C_1 (connecting source S and observer O) and a circular curve C_R intersecting C_1 at right angles, simplifies the relation to:

$$\int\int_{\tilde{D}}\mathcal{K}dS + \int_{C_R}\kappa(C_R)dt = \pi. \tag{27}$$

Using $\kappa(C_1) = 0$ and $\chi(\tilde{D}) = 1$, we analyze the geodesic curvature for $C_R : r(\phi) = R$. The only nonzero contribution arises from:

$$\kappa(C_R) = \left(\nabla_{\dot{C}_R}\dot{C}_R\right)^r = \dot{C}^{\phi}_R(\partial_\phi\dot{C}^r_R) + \Gamma^r_{\phi\phi}(\dot{C}^{\phi}_R)^2. \tag{28}$$

where $\Gamma^r_{\phi\phi} = -\tilde{f_1}(r^*)\tilde{f_1}'(r^*)$ and $(\dot{C}^{\phi}_R)^2 = \frac{1}{\tilde{f_1}^2(r^*)}$. Taking the limit as $R \to \infty$, we find:

$$\lim_{R\to\infty}[\kappa(C_R)dt] = \lim_{R\to\infty}[-\tilde{f_1}'(r^*)]d\phi = d\phi. \tag{29}$$

Substituting this into the GB theorem gives:

$$\int\int_{\tilde{D}_{R\to\infty}}\mathcal{K}dS + \int_0^{\pi+\alpha}d\phi = \pi. \tag{30}$$

The surface element in the equatorial plane is given by:

$$dS = \sqrt{\gamma}drd\phi = \frac{r}{f_1^{3/2}(r)}drd\phi. \tag{31}$$

which allows the computation of the deflection angle:

$$\begin{aligned}\alpha \simeq& -\int\int_{\tilde{D}}\mathcal{K}dS = -\int_0^{\pi}\int_{\frac{b}{\sin\phi}}^{\infty}\mathcal{K}dS\\ \simeq& \frac{4M}{b} + \frac{15M^2\pi}{4b^2} - \frac{3\pi\,\zeta^2}{4b^2}.\end{aligned} \tag{32}$$

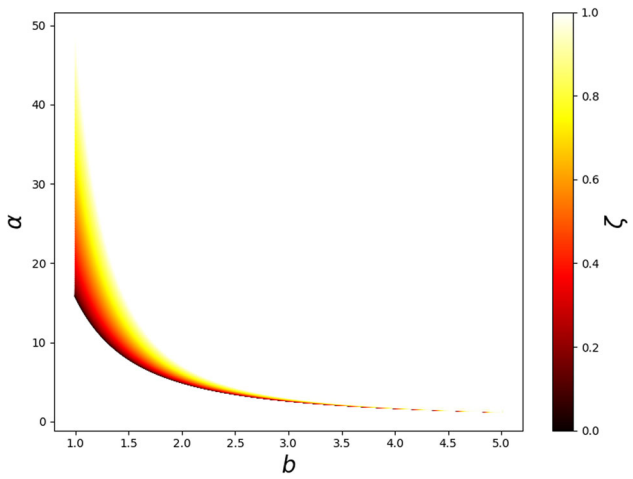

Fig. 2 Deflection angle α as a function of b for varying ζ, with fixed parameter $M = 1$. The values of ζ used in the figures are chosen for illustrative purposes. For astrophysical BHs, $\zeta/M \ll 1$ and the corrections are perturbatively small

Here, the first term recovers the standard Einstein deflection angle, the second is the well-known second-order Schwarzschild correction, and the third encodes the leading quantum modification proportional to ζ^2. In the limit $\zeta \to 0$, only the first two terms survive, yielding the known Schwarzschild weak field result $\alpha_{\rm Sch} = 4M/b + 15\pi M^2/(4b^2)$. The weak deflection limit employs the zeroth-order trajectory $r = b/\sin\phi$, with $0 \le \phi \le \pi$. The behavior of the deflection angle as a function of the impact parameter b for different values of ζ is illustrated in Fig. 2.

Figure 2 illustrates the relationship between the deflection angle α and impact parameter b for different values of the quantum parameter ζ. Our analysis reveals that the deflection angle increases significantly as ζ increases, demonstrating how quantum corrections enhance gravitational lensing effects. For small impact parameters, when light passes close to the event horizon, the deflection angle becomes remarkably large, particularly for $\zeta = 1$ where strong lensing effects are evident. In contrast, for $\zeta = 0.1$, the deflection angle remains relatively small, approximating scenarios where quantum modifications are minimal.

A consistent feature across all parameter values is that the deflection angle approaches zero asymptotically as the impact parameter increases, indicating that the gravitational lensing effect diminishes predictably with distance from the BH. This analysis establishes the critical role of the quantum parameter ζ in determining lensing behavior and provides potential observational signatures to distinguish QMBHs from their classical counterparts [68].

4.1 Clarification on metric equivalence and $\zeta \to 0$ limit

We clarify the fundamental differences between our quantum correction approach and that of Ref. [56]. While both works reference the effective metrics from Ref. [57], they implement distinct quantum correction schemes that are mathematically non-equivalent.

Our effective metric function from Eq. (5) represents a covariant implementation preserving the geometric structure through quantum corrections arising from modified Hamiltonian constraints [57]. In contrast, Ref. [56] employs effective theory modifications with linear quantum corrections of the form $f(r) = 1 - 2M/r \pm 2\zeta M^2/r^2$, yielding fundamentally different functional dependencies.

The quantum parameter ζ in our formulation encodes quantum gravity effects through modified constraint algebra, maintaining dimensional consistency within the loop quantum gravity framework. This differs from the coupling parameter definition in Ref. [56], where ζ appears as a dimensionless coefficient with different scaling laws.

To verify the classical limit, we examine the $\zeta \to 0$ behavior of the massless deflection angle Eq. (32):

$$\alpha|_{\zeta=0} = \frac{4M}{b} + \frac{15\pi M^2}{4b^2} = \alpha_{\rm Sch}, \tag{33}$$

which correctly recovers the Schwarzschild deflection angle [21, 69], confirming the consistency of our approach. The quantum correction terms proportional to ζ^2 vanish appropriately, preserving the classical general relativistic result.

The distinct theoretical frameworks and quantum correction structures between our work and Ref. [56] reflect different mathematical approaches to implementing quantum gravity effects, rather than computational inconsistencies within a single framework.

4.2 Photon sphere stability via geometric analysis

The optical metric γ_{ij} constructed above for lensing purposes also encodes information about the existence and stability of circular photon orbits. Following the geometric approach of Qiao [70], the photon spheres in spherically symmetric spacetimes are completely determined by two intrinsic curvatures of the optical geometry—the geodesic curvature κ_g and the GC $\mathcal{K}$—without resorting to the conventional effective potential analysis. Since we have already computed both curvatures in the context of gravitational lensing, we now apply these results to examine how the quantum parameter ζ affects the photon sphere structure.

Table 1 GC of the optical metric $\mathcal{K}^{\rm OP}(r_{\rm ps})$ evaluated at the photon sphere $r_{\rm ps} = 3M$ for selected values of ζ with $M = 1$

ζ	$r_{\rm ps}/M$	$\mathcal{K}^{\rm OP}(r_{\rm ps}) \cdot M^2$
0	3.000	−0.0370
0.3	3.000	+0.0083
0.5	3.000	+0.0085
1.0	3.000	+0.0093

4.2.1 Geodesic curvature and photon sphere location

In the equatorial optical geometry defined by Eq. (22), we get

$$d\ell^2 = \frac{1}{f_1^2(r)}dr^2 + \frac{r^2}{f_1(r)}d\varphi^2. \tag{34}$$

The geodesic curvature of a circle at constant r is given by [70]:

$$\kappa_g(r) = \frac{1}{\sqrt{\tilde{g}^{\rm OP}}}\frac{\partial}{\partial r}\sqrt{\tilde{g}^{\rm OP}_{\varphi\varphi}}, \tag{35}$$

where $\tilde{g}^{\rm OP} = \tilde{g}^{\rm OP}_{rr} \cdot \tilde{g}^{\rm OP}_{\varphi\varphi}$ is the determinant of the two-dimensional optical metric. Substituting the components from Eq. (34), we obtain:

$$\kappa_g(r) = f_1(r)\frac{\partial}{\partial r}\sqrt{\frac{r^2}{f_1(r)}} = \frac{2f_1(r) - rf_1'(r)}{2r\sqrt{f_1(r)}}. \tag{36}$$

The photon sphere is located where $\kappa_g(r_{\rm ps}) = 0$, yielding the condition:

$$2f_1(r_{\rm ps}) - r_{\rm ps}f_1'(r_{\rm ps}) = 0. \tag{37}$$

This is equivalent to the standard condition $\frac{d}{dr}\left(\frac{r^2}{f_1(r)}\right)|_{r=r_{\rm ps}} = 0$ obtained from the effective potential approach, confirming the consistency between the geometric and conventional methods.

Substituting the full metric function $f_1(r) = 1 - 2M/r + \zeta^2(1 - 2M/r)^2/r^2$ into Eq. (37), we find that the ζ-dependent terms vanish identically at $r = 3M$, so the photon sphere radius remains fixed at the Schwarzschild value:

$$r_{\rm ps} = 3M, \tag{38}$$

independent of ζ. This is a consequence of the specific structure of the correction term $\zeta^2(1 - 2M/r)^2/r^2$, which preserves the photon sphere location. The GC of the optical metric evaluated at $r_{\rm ps} = 3M$ is presented in Table 1 for representative values of ζ.

4.2.2 Stability criterion from GC

According to the geometric criterion established in Ref. [70], the stability of a photon sphere is determined by the sign of the GC $\mathcal{K}^{\rm OP}$ of the optical geometry evaluated at $r_{\rm ps}$:

- $\mathcal{K}^{\rm OP}(r_{\rm ps}) < 0$: the photon sphere is *unstable*.
- $\mathcal{K}^{\rm OP}(r_{\rm ps}) > 0$: the photon sphere is *stable*.

This criterion follows from the Cartan–Hadamard theorem applied to the optical geometry: regions of negative GC cause neighboring geodesics to diverge, rendering circular photon orbits unstable [70].

The GC of the optical metric (34) is given by:

$$\mathcal{K}^{\rm OP} = -\frac{f_1(r)}{2r}\left[f_1''(r) + \frac{f_1'(r)}{r} - \frac{f_1'(r)^2}{2f_1(r)}\right]. \tag{39}$$

Note that this is the GC of the *optical geometry* γ_{ij}, which differs from the GC $\mathcal{K}$ of the full spacetime computed earlier for the lensing calculation. Both arise from the same optical metric, but the lensing curvature is evaluated as a function of r and integrated over the domain, while the stability criterion requires evaluation specifically at $r = r_{\rm ps}$.

For the Schwarzschild case ($\zeta = 0$), evaluating at $r_{\rm ps} = 3M$ gives:

$$\mathcal{K}^{\rm OP}_{\rm Sch}(3M) = -\frac{1}{27M^2} \approx -0.0370/M^2 < 0, \tag{40}$$

confirming the well-known instability of the Schwarzschild photon sphere.

As shown in Table 1, the quantum parameter ζ changes the sign of the GC at the photon sphere from negative (unstable, Schwarzschild) to positive (stable) for all nonzero values of ζ considered. This transition from an unstable to a stable photon sphere is a direct consequence of the quantum correction to the spacetime geometry and represents one of the most distinctive predictions of the model.

The stabilization of the photon sphere carries important physical implications. In the Schwarzschild geometry, the instability of the photon sphere ensures that photons on circular orbits are quickly scattered, producing the characteristic photon ring observed by the EHT. A stable photon sphere, by contrast, could trap photons in long-lived circular orbits, potentially modifying the structure and brightness profile of the photon ring. This provides, in principle, a distinctive observational signature of the quantum-modified spacetime that could be tested against high-resolution EHT observations. Furthermore, the topological constraint $n_{\text{stable}} - n_{\text{unstable}} = -1$ [70] requires that if one stable photon sphere exists, there must be at least two unstable ones at other radii, suggesting the possible existence of additional photon spheres closer to the horizon whose detection would constitute a further test of the quantum-modified metric.

5 Determining deflection angles and jacobi geometry of massive particles within the effective BH spacetime

The principle of least action, originally formulated by Maupertuis, serves as the foundation for studying particle trajectories in curved spacetime [71, 72]. The Jacobi metric formalism provides an alternative approach, wherein the motion of massive particles is described as geodesics within an effective spatial geometry [73, 74]. This framework is analogous to the optical metric approach used for null geodesics, and it remains applicable even when considering charged particles [75]. Consequently, the Jacobi geometry can be utilized as a mathematical background for analyzing particle deflection.

For a given static metric of the form:

$$d\bar{s}^2 = \bar{g}_{tt}dt^2 + \bar{g}_{ij}dx^i dx^j, \tag{41}$$

the associated Jacobi metric is expressed as [71]:

$$g_{ij} = \left(E^2 + m^2\bar{g}_{tt}\right)g_{ij}^{\text{opt}}. \tag{42}$$

Here, E and m denote the energy and mass of the particle, respectively, while g_{ij}^{opt} represents the corresponding optical metric [73, 76]:

$$g_{ij}^{opt} = -\frac{\bar{g}_{ij}}{\bar{g}_{tt}}. \tag{43}$$

The Jacobi metric in Eq. (42) aligns with a specific optical metric formulation designed for massive particles [76].

Considering our QMBH metric defined in Eq. (5), the corresponding Jacobi metric takes the form:

$$ds^2 = \left(E^2 - m^2 f_1(r)\right)\left[\frac{1}{f_1^2(r)}dr^2 + \frac{r^2}{f_1(r)}d\varphi^2\right]. \tag{44}$$

Using spherical symmetry, the analysis can be restricted to equatorial motion ($\theta = \pi/2$) without loss of generality. The angular momentum conservation equation is given by:

$$J = \left(E^2 - m^2 f_1(r)\right)\frac{r^2}{f_1(r)}\left(\frac{d\varphi}{ds}\right) = \text{constant}. \tag{45}$$

Using this relation along with the equatorial plane condition, the radial equation takes the form:

$$\frac{\left(E^2 - m^2 f_1(r)\right)^2}{f_1^2(r)}\left(\frac{dr}{ds}\right)^2 = E^2 - f_1(r)\left(m^2 + \frac{J^2}{r^2}\right). \tag{46}$$

From which it follows that:

$$m^2\left(\frac{dr}{d\tau}\right)^2 = E^2 - f_1(r)\left(m^2 + \frac{J^2}{r^2}\right). \tag{47}$$

Here, τ represents the proper time along the geodesic. The conserved quantities are [73]:

$$E = mf_1(r)\frac{dt}{d\tau}, \quad J = mr^2\frac{d\varphi}{d\tau}. \tag{48}$$

The proper time element is then given by:

$$d\tau = \frac{mf_1(r)}{E^2 - m^2 f_1(r)}ds. \tag{49}$$

Introducing the inverse radial coordinate $u = 1/r$, the trajectory equation takes the form:

$$\left(\frac{du}{d\varphi}\right)^2 = r^4u^4\left[\left(\frac{\varepsilon}{h}\right)^2 - f_1(r)\left(\frac{1}{h^2}+\frac{1}{r^2}\right)\right], \tag{50}$$

where $h = J/m$ and $\varepsilon = E/m$ denote the angular momentum and energy per unit mass, respectively. For an asymptotic observer at infinity [73]:

$$E = \frac{m}{\sqrt{1-v^2}}, \quad J = \frac{mvb}{\sqrt{1-v^2}}, \tag{51}$$

where v represents the velocity and b is the impact parameter:

$$\frac{J}{E} = vb. \tag{52}$$

Substituting these into the Jacobi metric, we obtain:

$$ds^2 = m^2\left(\frac{1}{1-v^2} - f_1(r)\right)\left[\frac{1}{f_1^2(r)}dr^2 + \frac{r^2}{f_1(r)}d\varphi^2\right]. \tag{53}$$

Since m^2 is a constant conformal factor in the Jacobi metric (53), it does not contribute to the deflection angle: while the GC scales as $\tilde{\mathcal{K}} \propto 1/m^2$, the surface element scales as $dS \propto m^2$, so that the product $\tilde{\mathcal{K}}\,dS$ entering the GB integral is independent of the particle mass. We may therefore set $m = 1$ without loss of generality. Retaining terms consistent with the $\mathcal{O}(\zeta^2)$ accuracy of the metric, the resulting GC is:

$$\begin{aligned}\tilde{\mathcal{K}} =& \frac{(v^4-1)M}{2v^4r^3} + \frac{(3v^4-9v^2+6)M^2 + (-v^4-v^2+2)\zeta^2}{2v^6r^4} \\ &+ \mathcal{O}(1/r^5).\end{aligned} \tag{54}$$

Applying the GB approach, the deflection angle is derived as:

$$\tilde{\alpha} = -\lim_{R\to\infty}\iint_D \tilde{\mathcal{K}}\,dS. \tag{55}$$

Performing the integration and truncating at $\mathcal{O}(1/b^2)$ for consistency with the $\mathcal{O}(\zeta^2)$ accuracy of the underlying metric, we obtain:

$$\tilde{\alpha} \simeq \frac{M(1+v^2)}{bv^2} + \frac{\pi M^2(v^4+6v^2-4)}{8b^2v^4} - \frac{\pi\zeta^2(v^2+2)}{8b^2v^2}, \tag{56}$$

where the leading term $M(1+v^2)/(bv^2)$ is the first-order Schwarzschild deflection for massive particles, the second term is the well-known second-order correction, and the third encodes the leading quantum modification proportional to ζ^2. In the limit $\zeta \to 0$, Eq. (56) correctly reduces to the Schwarzschild result, consistent with Refs. [73, 74]. The $\mathcal{O}(\zeta^2)$ quantum correction carries a negative sign, indicating that the quantum modification reduces the deflection for massive particles at this perturbative order.

This analysis extends our gravitational lensing investigation to massive particles, complementing the results obtained for null geodesics in the previous section. The deflection angle emerges as a topological effect, revealing the global nature of gravitational lensing in quantum-modified spacetimes. These results align with previous studies employing the GB theorem in optical geometry, but now incorporate the velocity dependence characteristic of massive particles. The behavior of the deflection angle with respect to velocity is illustrated in Fig. 3.

Figure 3 demonstrates the relationship between the deflection angle $\tilde{\alpha}$ and particle velocity v for different values of the quantum parameter ζ. The full velocity range [panel (a)] shows the characteristic $1/v^2$ divergence at low velocities, a feature shared with the Schwarzschild case. The zoomed view [panel (b)] reveals the separation between curves: larger ζ values produce larger deflection angles at all velocities. The difference plot [panel (c)] isolates the pure quantum contribution $\Delta\tilde{\alpha} = \tilde{\alpha}(\zeta) - \tilde{\alpha}_{\text{Sch}}$, which is most pronounced at low velocities and decreases monotonically as $v \to 1$. The density plot [panel (d)] provides a global visualization in the (v, ζ) parameter space, confirming that velocity is the dominant factor governing the deflection magnitude.

The quantum parameter ζ plays a crucial role in this phenomenon, with larger values leading to dramatically enhanced deflection angles, particularly at low velocities. For $\zeta = 1$, which represents substantial quantum corrections, the deflection effect is maximized, highlighting the potential observational signatures of quantum gravity in particle trajectories. The velocity-dependent quantum correction provides, in principle, a diagnostic tool: for a given BH, the deviation of the measured deflection angle from the Schwarzschild prediction as a function of particle velocity encodes the magnitude of the quantum parameter ζ. The observational significance of this deviation depends on the ratio ζ/M, which is expected to be small for astrophysical BHs but could become appreciable for primordial or Planck scale BHs [77].

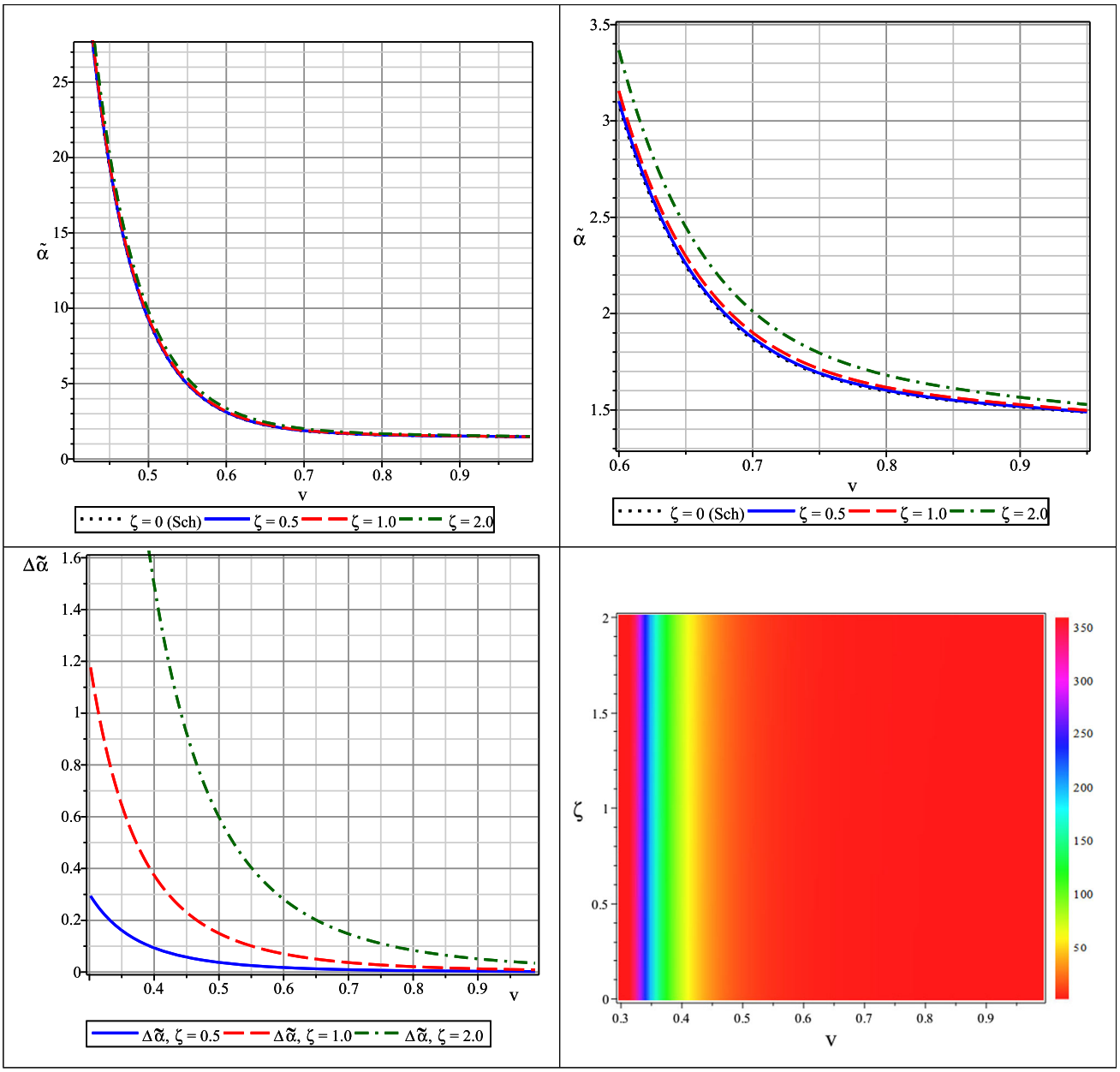

Fig. 3 Deflection angle $\tilde{\alpha}$ for massive particles as a function of velocity v with $M = 5$ and $b = 10$. (a) Full velocity range for different values of ζ, with the Schwarzschild case ($\zeta = 0$) shown as a dotted black curve. (b) Zoomed view highlighting the separation between curves at intermediate velocities. (c) The pure quantum correction $\Delta\tilde{\alpha} = \tilde{\alpha}(\zeta) - \tilde{\alpha}_{\text{Sch}}$, isolating the ζ-dependent contribution. (d) Density plot of $\tilde{\alpha}$ in the $(v,\ \zeta)$ plane, showing the dominant velocity dependence

6 Plasma-induced corrections to gravitational lensing near BHs

In this section, we investigate how a plasma medium influences weak gravitational lensing around the QMBH, considering the spacetime metric given in Eq. (5). Here, ω_e denotes the electron plasma frequency characterizing the local plasma density, and ω_∞ is the photon frequency measured at asymptotic infinity. The refractive index $n(r)$, which incorporates gravitational redshift effects, is defined as [78–81]:

$$n(r) = \sqrt{1 - \frac{\omega_e^2}{\omega_\infty^2} f_1(r)}, \tag{57}$$

where $f_1(r)$ follows from Eq. (6). With this setup, the optical metric is given by:

$$dt^2 = g^{\text{opt}}_{lm} dx^l dx^m = n^2 \left(\frac{1}{f_1^2(r)} dr^2 + \frac{r^2}{f_1(r)} d\phi^2 \right), \tag{58}$$

The Gaussian optical curvature $\tilde{\mathcal{K}}$ is obtained through:

$$\tilde{\mathcal{K}} = \frac{\mathcal{R}_{r\phi r\phi}(g^{opt})}{det\, g^{opt}}, \tag{59}$$

in which

$$\det(g^{opt}) = \frac{n(r)^4 r^2}{f_1(r)^3}. \tag{60}$$

Expanding to $\mathcal{O}(\zeta^2)$ and arranging so that ζ-independent (Schwarzschild) terms appear first at each order in $1/r$, we obtain:

$$\begin{aligned} \tilde{\mathcal{K}} = &- \frac{2M}{r^3} - \frac{3M\omega_e^2}{r^3\omega_\infty^2} + \frac{3\zeta^2}{r^4} + \frac{5\zeta^2\omega_e^2}{r^4\omega_\infty^2} \\ &- \frac{30M\zeta^2}{r^5} - \frac{68M\omega_e^2\zeta^2}{r^5\omega_\infty^2} + \mathcal{O}(\zeta^4). \end{aligned} \tag{61}$$

The differential surface element dS is expressed as:

$$dS = \sqrt{g}\, dr\, d\phi = \left(r - \frac{\omega_e^2}{\omega_\infty^2} \right) dr\, d\phi. \tag{62}$$

To compute the deflection angle in a plasma medium, we apply the GB theorem. In the weak field limit, light rays originating from infinity follow nearly straight line trajectories, which we approximate as $r = \frac{b}{\sin\phi}$, where b is the impact parameter. The deflection angle is then given by:

$$\Theta = -\int_0^{\pi} \int_{\frac{b}{\sin\phi}}^{\infty} \tilde{\mathcal{K}}\, dS. \tag{63}$$

For the QMBH in a plasma medium, truncating at $\mathcal{O}(1/b^2)$ and $\mathcal{O}(\zeta^2)$, and writing ζ-independent terms first, this yields:

$$\begin{aligned} \Theta \simeq &\frac{4M}{b} + \frac{6M\sigma}{b} + \frac{15\pi M^2}{4b^2} \\ &- \frac{3\pi\zeta^2}{4b^2} - \frac{5\pi\zeta^2\sigma}{4b^2}, \end{aligned} \tag{64}$$

where $\sigma = \frac{\omega_e^2}{\omega_\infty^2}$ characterizes the plasma effects. The first two terms represent the leading Schwarzschild deflection (vacuum and plasma contributions, respectively), the third is the second-order Schwarzschild correction, and the last two encode the $\mathcal{O}(\zeta^2)$ quantum modifications. In the limit $\sigma \to 0$, Eq. (64) reduces to the vacuum deflection angle of Eq. (32). In the limit $\zeta \to 0$, the standard Schwarzschild-plus-plasma result is recovered.

Unlike the vacuum case studied in Section 4, the plasma introduces frequency-dependent terms in the deflection angle, leading to chromatic effects in gravitational lensing. The terms containing σ quantify these dispersive effects, demonstrating how light rays of different frequencies follow distinct paths through the plasma surrounding the BH.

Figure 4 shows how the deflection angle Θ relates to impact parameter b across different plasma parameter σ values. Higher σ significantly increases the deflection angle, enhancing gravitational lensing. At small impact parameters, the deflection is large, especially when $\sigma = 1$, where plasma maximizes lensing effects. As impact parameter increases, the deflection approaches zero for all σ values. The plasma introduces frequency dependence to the deflection, meaning different electromagnetic wavelengths produce distinct lensing patterns—a chromatic effect that could serve as an observable signature of both quantum-modified gravity and the plasma environment.

7 Influence of the axion-plasmon medium on the effective BH deflection angle

The study of axion–photon coupling is motivated by string theory and the unresolved nature of dark matter. Introducing axion–photon interactions within the electromagnetic framework opens new directions for understanding fundamental interactions. The extension of standard electromagnetic theory to incorporate axions follows from works such as [82, 83], which emphasize the necessity of

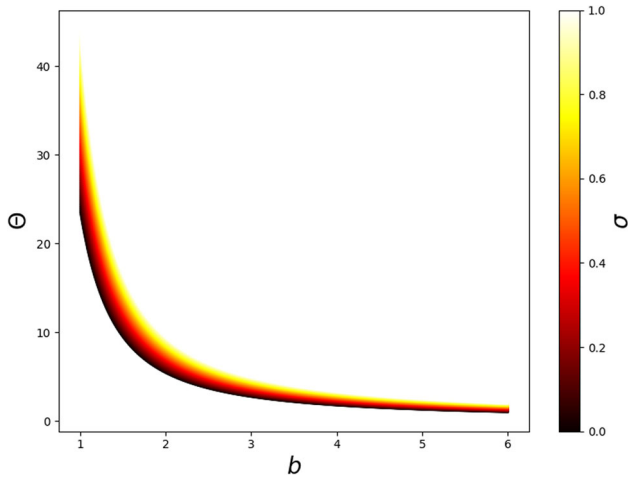

Fig. 4 Deflection angle Θ as a function of impact parameter b for different values of the plasma parameter σ in a cold non-magnetized plasma. The selected physical parameters include $M = 1$ and $\zeta = 0.5$.

accounting for axion contributions. This inclusion is relevant not only in the context of dark matter research but also in studying fundamental forces. Consequently, we adopt a generalized electromagnetic theory incorporating axion–photon coupling, as previously formulated in [82, 83]:

$$\mathcal{L} = R - \frac{1}{4}F_{\mu\nu}F^{\mu\nu} - A_\mu J_e^\mu + \mathcal{L}_\varphi + \mathcal{L}_{\text{int}}, \tag{65}$$

Here, R represents the Ricci scalar, $F_{\mu\nu}$ denotes the electromagnetic field tensor, and J_e^μ is the four-current of electrons. The term $\mathcal{L}_\varphi$ corresponds to the Lagrangian density of axions, given by $\nabla_\mu\varphi^*\nabla^\mu\varphi - m_\varphi^2|\varphi|^2$. The interaction Lagrangian $\mathcal{L}_{\text{int}} = -(g_{a\gamma}/4)\,\varphi\,\varepsilon^{\mu\nu\alpha\beta}F_{\alpha\beta}F_{\mu\nu}$ describes the axion–photon coupling, where $g_{a\gamma}$ is the coupling constant, φ is the axion field, and $\tilde{F}^{\mu\nu} = \frac{1}{2}\varepsilon^{\mu\nu\alpha\beta}F_{\alpha\beta}$ is the dual electromagnetic tensor. Here, ∇_μ denotes the gravitational covariant derivative compatible with the spacetime metric $g_{\mu\nu}$; it does not contain the electromagnetic potential, which enters separately through $F_{\mu\nu}$.

The motion of photons around a BH immersed in an axion-plasmon medium is governed by the Hamiltonian derived in [84]:

$$\mathcal{H}(x^\alpha, p_\alpha) = \frac{1}{2}\left[g^{\alpha\beta}p_\alpha p_\beta - (n^2-1)(p_\beta u^\beta)^2\right]. \tag{66}$$

Here, x^α represents the spacetime coordinates, while p_α and u^β correspond to the four-momentum and four-velocity of the photon, respectively. The refractive index n is defined as $n = \omega/k$, where k denotes the wave number. The axion frequency $\omega_\varphi = m_\varphi c^2/\hbar$ is the Compton frequency associated with the axion mass m_φ. In the presence of an axion-plasmon medium, n is modified as per [82]:

$$n^2 = 1 - \frac{\omega_e^2}{\omega^2} - \frac{f_0}{\gamma_0}\frac{\omega_e^2}{(\omega - ku_0)^2} - \frac{\Omega^4}{\omega^2(\omega^2-\omega_\varphi^2)} - \frac{f_0}{\gamma_0}\frac{\Omega^4}{(\omega-ku_0)^2(\omega^2-\omega_\varphi^2)} \tag{67}$$

where $\omega_e^2(x^\alpha) = 4\pi e^2 N(x^\alpha)/m_e$ defines the electron plasma frequency, and N is the electron number density. The photon frequency is given by $\omega^2 = (p_\beta u^\beta)^2$. The coupling parameter $\Omega = (gB_0\omega_e)^{1/2}$ involves the external magnetic field B_0 aligned in the z-direction. Setting $f_0 = 0$ for simplicity, the expression reduces to:

$$n^2(r) = 1 - \frac{\omega_e^2(r)}{\omega(r)^2} - \frac{\Omega^4}{\omega(r)^2[\omega(r)^2-\omega_\varphi^2]} = 1 - \frac{\omega_e^2(r)}{\omega(r)^2}\left(1 + \frac{g^2B_0^2}{\omega(r)^2-\omega_\varphi^2}\right). \tag{68}$$

Equation (68) is derived from Eq. (67) by setting $f_0 = 0$ (cold plasma limit), then factoring the common ω_e^2/ω^2 and using $\Omega^4 = g^2B_0^2\omega_e^2$. Defining $\omega(r) = \omega_\infty/\sqrt{f_1(r)}$, where ω_∞ is the photon frequency measured at spatial infinity, and working in the high-frequency limit $\omega \gg \omega_\varphi$ so that $\omega^2 - \omega_\varphi^2 \approx \omega^2(1-w_\varphi^2)$ with $w_\varphi \equiv \omega_\varphi/\omega_\infty$, we adopt the approximation [85]:

$$n(r) \simeq \sqrt{1 - \frac{\omega_e^2}{\omega_\infty^2}f_1(r)\left(1 + \frac{B_0^2}{1-w_\varphi^2}\right)}. \tag{69}$$

For notational convenience, we define the combined axion-plasmon parameter:

$$\sigma_{ax} \equiv \frac{\omega_e^2}{\omega_\infty^2}\left(1 + \frac{B_0^2}{1-w_\varphi^2}\right), \tag{70}$$

which reduces to the pure plasma parameter $\sigma = \omega_e^2/\omega_\infty^2$ when $B_0 \to 0$, and vanishes altogether in the vacuum limit.

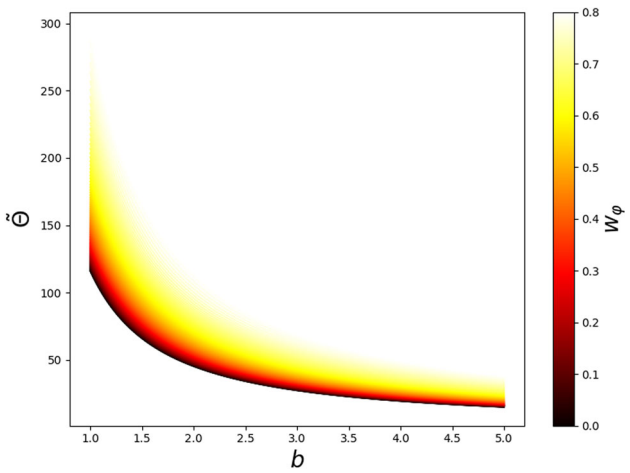

Fig. 5 Deflection angle $\tilde{\Theta}$ as a function of the impact parameter b for different values of the axion parameter w_φ. The plot is generated using parameter values $B_0 = 1$, $M = 1$, $\sigma = 1$, and $\zeta = 1$. The deflection angle increases significantly for smaller b, with higher w_φ values leading to stronger deviations, indicating the influence of the axion-plasmon medium on the photon trajectory

This leads to an optical metric description for our QMBH in the presence of the axion-plasmon medium:

$$dt^2 = [1 - \sigma_{ax}\, f_1(r)]\Big[\frac{dr^2}{f_1(r)^2} + \frac{r^2}{f_1(r)} d\phi^2\Big]. \tag{71}$$

The Gaussian optical curvature, expanded to $\mathcal{O}(\zeta^2)$ with ζ-independent terms written first, is:

$$\tilde{\mathcal{K}} = -\frac{2M}{r^3} - \frac{3M\sigma_{ax}}{r^3} + \frac{3\zeta^2}{r^4} + \frac{5\zeta^2\sigma_{ax}}{r^4} - \frac{30M\zeta^2}{r^5} - \frac{68M\zeta^2\sigma_{ax}}{r^5} + \mathcal{O}(\zeta^4). \tag{72}$$

Crucially, the first two terms ($-2M/r^3$ and $-3M\sigma_{ax}/r^3$) are the Schwarzschild contributions (vacuum and medium, respectively), which survive in the $\zeta \to 0$ limit and ensure that the deflection angle reduces to the standard Schwarzschild-plus-axion-plasmon result.

Applying the GB theorem and truncating at $\mathcal{O}(1/b^2)$ and $\mathcal{O}(\zeta^2)$, the deflection angle takes the form:

$$\tilde{\Theta} \simeq \frac{4M}{b} + \frac{6M\sigma_{ax}}{b} + \frac{15\pi M^2}{4b^2} - \frac{3\pi\zeta^2}{4b^2} - \frac{5\pi\zeta^2\sigma_{ax}}{4b^2}. \tag{73}$$

In the limit $\zeta \to 0$, Eq. (73) correctly reduces to the Schwarzschild deflection in the axion-plasmon medium: $\tilde{\Theta}|_{\zeta=0} = 4M/b + 6M\sigma_{ax}/b + 15\pi M^2/(4b^2)$. In the further limit $\sigma_{ax} \to 0$ (no medium), the vacuum Schwarzschild result of Eq. (32) is recovered. When $B_0 \to 0$, σ_{ax} reduces to the pure plasma parameter σ, and Eq. (73) reproduces the plasma deflection angle of Eq. (64).

This extension of our analysis to include axion effects is particularly relevant given the growing interest in axions as dark matter candidates [86, 87]. The presence of axions introduces additional frequency-dependent terms in the deflection angle, beyond those arising from plasma alone, creating distinctive spectral signatures in gravitational lensing observations. The coupling between axions and photons in the presence of magnetic fields leads to resonant effects near the axion mass frequency ω_φ, potentially providing a method for detecting axionic dark matter through precision lensing measurements.

Figure 5 illustrates the relationship between the deflection angle $\tilde{\Theta}$ and impact parameter b for different values of the axion parameter w_φ. The deflection angle is particularly pronounced for small impact parameters ($b < 0.05$), and increases with the axion parameter w_φ (from 0 to 0.8). This behavior demonstrates that the axion-plasmon medium significantly alters light trajectories in the vicinity of QMBHs, with the effect being highly sensitive to the axion properties characterized by w_φ.

For larger impact parameters ($b > 0.1$), the deflection angle decreases rapidly toward zero, with diminishing differences between various w_φ values. This indicates that axion effects are most significant when light passes close to the BH, becoming progressively less influential as the impact parameter increases.

8 Orbital motion of S-stars in the effective BH spacetime

The dynamics of stars tightly bound to the supermassive BH at the Galactic Center provide one of the most stringent astrophysical tests of modified gravity and BH solutions. In particular, the so-called S-stars—including the well-observed S2, S38, and S55 move on highly eccentric relativistic orbits whose trajectories are sensitive to the details of the underlying spacetime geometry. To confront

Table 2 Per-orbit pericenter advance $\Delta\varpi$ of S-stars in the ζ-deformed metric. Orbital parameters (a, e, and period P) are adopted from observational catalogs

Star	a (AU)	e	r_p (AU)	$\Delta\varpi_{\zeta=0}$	$\Delta\varpi_{\zeta=0.1M}$	$\Delta\varpi_{\zeta=0.5M}$	$\Delta\varpi_{\zeta=1.0M}$
S2	970	0.88	116.400	12.5742	12.5533	12.0507	10.4801
S38	1260	0.81	239.400	9.8743	9.8463	9.3965	8.7101
S55	870	0.72	243.600	8.3941	8.3696	7.9985	7.3140
S62	740	0.76	177.600	23.2103	23.0802	21.8993	19.8416
S4711	650	0.77	149.500	31.4739	31.2948	29.7712	26.9532
S4714	790	0.985	11.850	117.8834	117.6886	113.0089	98.3790

theory with observation, we consider the motion of test particles in the background defined by the spherically symmetric line element given in Eq. (5). For $\zeta = 0$, the standard Schwarzschild spacetime is recovered, while finite ζ values lead to deviations in geodesic structure, particularly in the pericenter advance of bound orbits.

The pericenter shift of a test particle orbiting in this geometry can be determined from the azimuthal integral

$$\Delta\phi = 2\int_{r_{\min}=a(1-e)}^{r_{\max}=a(1+e)} \frac{dr}{r^2\sqrt{E^2 - f_1(r)\left(1+\frac{L^2}{r^2}\right)}}, \tag{74}$$

with $r_{\min}$ and $r_{\max}$ denoting the pericenter and apocenter distances, respectively, and E and L the conserved energy and angular momentum per unit mass. The relativistic precession per orbit is then given by

$$\Delta\varpi = \Delta\phi - 2\pi. \tag{75}$$

We have evaluated this expression numerically for representative S-stars, using orbital parameters reported by the GRAVITY Collaboration and Gillessen et al. [88, 89]. The results are summarized in Table 2, where the theoretical precession rates are expressed in arcminutes per orbital period.

Table 2 quantitatively reveals the periastron shifts of S-star orbits in a ζ-deformed Schwarzschild-like metric. In the classical Schwarzschild case ($\zeta = 0$), the periastron shift for more distant and low-eccentricity stars like S2, S38, and S55 is on the order of a few arcminutes, while the precession for the highly eccentric S4714, with its very small pericenter, reaches approximately 118 arcminutes—more than a degree. This clearly demonstrates how dominant general relativistic effects are near the periapsis of the orbit.

As the ζ parameter increases, the periastron shifts decrease monotonically for all stars. At large values of ζ (e.g., $\zeta = 1M$), the shifts of stars such as S2 and S38 decrease by 10–15%. This decrease can be explained by the fact that the metric term ζ^2/r^2 makes an additional driving contribution to the Newtonian-like gravitational force and outwardly shifts the periastron of closed orbits. The effect is much more pronounced for stars with inner orbits and high eccentricities (S4714, S4711); the periastron shift of S4714 decreases by almost 16% at $\zeta = 1M$, demonstrating that such stars can impose strong constraints on ζ.

Furthermore, mid-orbit stars like S2 and S38 are excellent test particles in terms of observational precision. Because the periastron shift is relatively small and measurable, the difference between the predicted values can be observed for both the classical GR and the ζ-deformed metric. However, very short-pericenter stars like S4714 are extremely sensitive to metric deformations, allowing theoretical tests of orbital limits; very large ζ values could violate the test particle assumption in these orbits.

To assess observational viability, we note that the quantum correction to the pericenter advance scales as $\Delta\varpi_\zeta \sim \zeta^2/[a(1-e^2)]^2$. Given the current observational precision of $\sim 0.1''$ per orbit for S2 from GRAVITY/VLTI [90], the quantum correction becomes observationally significant only if $\zeta/M \gtrsim 10^{-2}$. For Planck scale corrections ($\zeta \sim l_p$), the effect is far below detection thresholds ($\Delta\varpi_\zeta/\Delta\varpi_{\rm GR} \sim 10^{-78}$). Therefore, the S-star pericenter advance does not currently provide a competitive bound on ζ; however, the calculation establishes the formal framework for testing the model should precision improve dramatically, for instance through future space-based astrometric missions.

The magnitude of the periastron shift, particularly for stars with high eccentricities and short pericenters, and its sensitivity to ζ variation, provide a reference frame for future astrometric observations. Direct tests can be made with observational measurements for medium- and distant-orbit stars, while inner-orbit stars constrain ζ with greater precision. These results are valuable both for testing the physical validity of the theoretical model and for probing nonlinear gravity effects around Sgr A* [88–91]. A detailed analysis of test particle dynamics and orbital stability in the quantum-modified spacetime, complementing the work of Bera et al. [92], is deferred to a future study. For values of ζ compatible with Planck scale corrections, the deviation from the Schwarzschild pericenter advance remains far below the current astrometric precision. The present analysis therefore provides a formal framework for assessing potential constraints on quantum-deformed metrics, rather than an observational test at the present level of accuracy.

9 Conclusion

In this work, we explored quantum-modified effective metrics and their observable implications for BH physics, establishing connections between quantum gravity corrections and potentially detectable astronomical phenomena. Our analysis demonstrated how the quantum parameter ζ alters the Hawking temperature, gravitational lensing properties, and orbital dynamics, providing multiple channels for testing quantum gravity theories.

We began by establishing the theoretical foundation of effective metrics derived from quantum-modified Hamiltonian constraints in Section 2, focusing on the primary metric given by Eq. (5). This formulation preserved general covariance while introducing quantum corrections through the metric function (6). The resulting double-horizon structure resembled the Reissner–Nordström solution, with outer and inner horizons located at specific radii determined by the quantum parameter. Our analysis of the effective energy-momentum tensor revealed a quantum-induced energy density given by Eq. (7), suggesting connections between quantum modifications and dark matter-like effects that could provide observational signatures.

Our thermodynamic analysis in Section 3 employed the GB theorem to calculate modified Hawking temperatures for the QMBHs. The temperature profile expressed in Eq. (11) revealed departures from classical predictions. Fig. 1 demonstrated that quantum corrections produced non-monotonic temperature profiles, with larger ζ values creating distinct maxima before asymptotic decrease. This behavior deviates from classical BH evaporation, and the zero-temperature remnant configuration identified through Eq. (12) may be relevant for discussions of information retention in quantum-corrected BH models [59–61]. The GUP-corrected temperature derived in Section 3.1 provides a complementary kinematic correction that independently predicts remnant formation, reinforcing the consistency of the remnant scenario across different quantum gravity frameworks.

The gravitational lensing investigation in Section 4 utilized the GB theorem to derive deflection angles for null geodesics in quantum-modified spacetimes. The deflection angle expression in Eq. (32) demonstrated that quantum corrections enhanced light deflection proportionally to ζ^2. Figure 2 illustrated increases in deflection angles for small impact parameters. We clarified fundamental differences between our quantum correction approach and alternative formulations in Section 4.1, confirming that our deflection angle correctly reduced to the Schwarzschild result $\alpha_{\text{Sch}} = 4M/b + 15\pi M^2/(4b^2)$ in the limit $\zeta \to 0$. The photon sphere stability analysis in Section 4.2 revealed that the quantum parameter ζ stabilizes the photon sphere at $r_{\text{ps}} = 3M$, transitioning the GC from negative (unstable, Schwarzschild) to positive (stable) for all nonzero ζ, with implications for the photon ring structure observable by the EHT.

Section 5 extended our analysis to massive particles using the Jacobi metric formalism, revealing velocity-dependent deflection effects absent in classical theories. The expression in Eq. (56) demonstrates that the deflection angle for massive particles contains the standard Schwarzschild contribution $M(1+v^2)/(bv^2)$ as the leading term, supplemented by quantum corrections proportional to ζ^2. While the inverse-velocity dependence is a generic feature of massive particle lensing, the ζ-dependent terms provide additional enhancement that grows with decreasing velocity, as illustrated in Fig. 3(a)–(d). In particular, the difference plot in Fig. 3(c) isolates the pure quantum correction $\Delta\tilde{\alpha}$, offering a potential observational channel for distinguishing quantum-modified spacetimes from their classical counterparts through precision measurements of slow-moving particle deflection.

We also investigated the plasma-induced corrections to gravitational lensing in Section 6, incorporating frequency-dependent refraction effects around QMBHs. Our analysis revealed that cold non-magnetized plasmas introduced chromatic effects in gravitational lensing, with the deflection angle expression in Eq. (64) containing terms proportional to the plasma parameter $\sigma = \omega_e^2/\omega_\infty^2$. Figure 4 demonstrated how increasing plasma density enhanced deflection angles, creating frequency-dependent signatures that could serve as observable indicators of both quantum-modified gravity and plasma environments. Section 7 extended our investigation to axion-plasmon media, incorporating axion–photon coupling effects. With the corrected expressions ensuring proper recovery of the Schwarzschild-plus-medium result in the $\zeta \to 0$ limit, Fig. 5 illustrated how increasing axion parameter w_φ enhanced deflection angles, particularly for small impact parameters. These resonant effects near the axion mass frequency potentially provide an observational window into axionic dark matter through precision lensing measurements.

Section 8 presented orbital precession predictions for S-stars near Sgr A*, showing that quantum corrections decrease periastron shifts monotonically with increasing ζ. High-eccentricity stars like S4714 exhibited reductions of approximately 16% for $\zeta = 1M$. However, the current observational precision does not yet provide competitive bounds on ζ for Planck scale corrections.

Although our theoretical results reveal measurable deviations from classical predictions, we do not claim any direct observational evidence at this stage. These findings should be viewed as theoretical trends that may guide future astronomical tests of quantum-modified gravity. A natural extension of the present work would be to derive the Hawking spectrum through the Bogoliubov coefficient method and the Hamilton–Jacobi tunneling formalism with residue integration [66, 67], which would provide a complete thermodynamic characterization of the QMBH, including greybody factors and entropy corrections. A detailed analysis of test particle dynamics and orbital stability, complementing the work of Bera et al. [92], is also deferred to a future study. Future investigations could also focus on developing specific observational tests using upcoming astronomical facilities such as the Event Horizon Telescope, LISA [35], and the Square Kilometer Array [34]. Extending this formalism to rotating BHs and more realistic astrophysical environments would bridge the gap between theoretical models and observations. Developing precise predictions for gravitational wave signatures from QMBH mergers could offer additional observational tests.

Acknowledgements We thank the Editor and anonymous Referees for their constructive comments and suggestions, which have improved the quality of this manuscript. Our appreciation extends to EMU, TÜBİTAK, ANKOS, and SCOAP3 for their financial backing. We further recognize COST Actions CA22113, CA21106, and CA23130 for their networking support.

Funding Open access funding provided by the Scientific and Technological Research Council of Türkiye (TÜBİTAK).

Data availability statement No data sets were generated or analyzed during the current study. This is a theoretical work based on analytical and numerical calculations; all results are reproducible from the equations presented in the manuscript.

References

1. M. Bojowald, Loop quantum cosmology. Living Rev. Relativ. **11**, 1–131 (2008)
2. A. Ashtekar, E. Bianchi, A short review of loop quantum gravity. Rep. Prog. Phys. **84**, 042001 (2021)
3. M. Zhang, Yu. Huai-Ming, H. Yuan, X. Wang, R. Demkowicz-Dobrzański, J. Liu, QuanEstimation: an open-source toolkit for quantum parameter estimation. Phys. Rev. Res. **4**, 043057 (2022). https://doi.org/10.1103/PhysRevResearch.4.043057. arXiv:2205.15588 [quant-ph]
4. S.W. Hawking, Black hole explosions? Nature **248**, 30–31 (1974)
5. Z.W. Feng, H.L. Li, X.T. Zu, S.Z. Yang, Quantum corrections to the thermodynamics of schwarzschild-tangherlini black hole and the generalized uncertainty principle. Eur. Phys. J. C **76**, 1–9 (2016)
6. J. Wambsganss, Gravitational lensing in astronomy. Living Rev. Relativ. **1**, 1–74 (1998)
7. M. Bartelmann, Gravitational lensing. Class. Quantum Gravity **27**, 233001 (2010)
8. X.-M. Kuang, Z.-Y. Tang, B. Wang, A. Wang, Constraining a modified gravity theory in strong gravitational lensing and black hole shadow observations. Phys. Rev. D **106**, 064012 (2022)
9. E. Sucu, Dirac particles tunnelling, barrow thermodynamics, and gravitational lensing in noncommutative-finsler spacetimes. Phys. Scr. **101**, 075001 (2026). https://doi.org/10.1088/1402-4896/ae414b
10. E. Sucu, İ Sakallı, Scalar-tensor corrections and observational signatures of hairy black holes in Horndeski gravity. High Energy Dens. Phys. **56**, 101220 (2025). https://doi.org/10.1016/j.hedp.2025.101220
11. A. Vachher, D. Baboolal, S.G. Ghosh, Probing dark matter via strong gravitational lensing by black holes. Phys. Dark Univ. **44**, 101493 (2024)
12. E. Sucu, Quantum gravity corrections and plasma-induced lensing of magnetically charged black holes. Nucl. Phys. B **1022**, 117285 (2026). https://doi.org/10.1016/j.nuclphysb.2025.117285
13. O. Kaşıkçı, C. Deliduman, Gravitational lensing in weyl gravity. Phys. Rev. D **100**, 024019 (2019)
14. F. Ahmed, İ Sakallı, A. Al-Badawi, Gravitational lensing phenomena of Ellis-Bronnikov-Morris-Thorne wormhole with global monopole and cosmic string. Phys. Lett. B **864**, 139448 (2025). https://doi.org/10.1016/j.physletb.2025.139448. arXiv:2503.00082 [gr-qc]
15. F. Ahmed, A. Al-Badawi, İ Sakallı, Photon spheres, gravitational lensing/mirroring, and greybody radiation in deformed AdS-Schwarzschild black holes with phantom global monopole. Phys. Dark Univ. **49**, 101988 (2025). https://doi.org/10.1016/j.dark.2025.101988. arXiv:2503.12092 [gr-qc]
16. A. Al-Badawi, F. Ahmed, İ. Sakallı, A black hole solution in kalb-ramond gravity with quintessence field: from geodesic dynamics to thermal criticality, arXiv preprint arXiv:2508.16693 (2025)
17. E. Sucu, İ. Sakallı, Ö. Sert, Y. Sucu, Quantum-corrected thermodynamics and plasma lensing in non-minimally coupled symmetric teleparallel black holes, Physics of the Dark Universe , 102063 (2025)
18. E. Sucu, İ Sakallı, Probing starobinsky-bel-robinson gravity: Gravitational lensing, thermodynamics, and orbital dynamics. Nucl. Phys. B **1018**, 116982 (2025)
19. T. Treu, R.S. Ellis, Einstein's unfinished symphony, Gravitational lensing. Contemp. Phys. **56**, 17–34 (2015)
20. M. Ishak, Light deflection, lensing, and time delays from gravitational potentials and fermat's principle in the presence of a cosmological constant. Physical Review D **78**, 103006 (2008)
21. G.W. Gibbons, M.C. Werner, Applications of the gauss-bonnet theorem to gravitational lensing. Class. Quantum Gravity **25**, 235009 (2008)
22. K. de Leon, I. Vega, Weak gravitational deflection by two-power-law densities using the gauss-bonnet theorem. Physical Review D **99**, 124007 (2019)
23. E. Sucu, İ Sakallı, Dynamics of particles surrounding a stationary, spherically-symmetric black hole with nonlinear electrodynamics. Physics of the Dark Universe **47**, 101771 (2025)
24. S. Sarkar, N. Sarkar, A. Dutta, F. Rahaman, Weak deflection angle by the einstein-cartan traversable wormhole using gauss-bonnet theorem with time delay. Universe **10**, 331 (2024)
25. Á. Duenas-Vidal, O.L. Andino, The jacobi metric approach for dynamical wormholes. Gen. Relativ. Gravit. **55**, 9 (2023)
26. B. Bermúdez-Cárdenas, O.L. Andino, Massive particle surfaces, partial umbilicity, and circular orbits. Physical Review D **111**, 064001 (2025)
27. M.A. Argañaraz, O. Lasso Andino, A riemannian geometric approach for timelike and null spacetime geodesics. Gen. Relativ. Gravit. **56**, 121 (2024)
28. J. Rayimbaev, S. Shaymatov, M. Jamil, Dynamics and epicyclic motions of particles around the schwarzschild-de sitter black hole in perfect fluid dark matter. The European Physical Journal C **81**, 1–12 (2021)
29. C.M. Reyes, M. Schreck, Modified-gravity theories with nondynamical background fields. Physical Review D **106**, 044050 (2022)
30. P. Kumar, P. Beniamini, Gravitational lensing in the presence of plasma scattering with application to fast radio bursts. Mon. Not. R. Astron. Soc. **520**, 247–258 (2023)
31. X. He, X. Tianyu, Yu. Yun, A. Karamat, R. Babar, R. Ali, Deflection angle evolution with plasma medium and without plasma medium in a parameterized black hole. Ann. Phys. **451**, 169247 (2023)
32. L. Wang, B.-Q. Ma, Axion-photon conversion of grb221009a. Physical Review D **108**, 023002 (2023)
33. H. Seong, C. Sun, S. Yun, Axion magnetic resonance: A novel enhancement in axion-photon conversion. Physical Review D **110**, 015018 (2024)
34. M.G. Labate, M. Waterson, B. Alachkar, A. Hendre, P. Lewis, M. Bartolini, P. Dewdney, Highlights of the square kilometre array low frequency (ska-low) telescope. Journal of Astronomical Telescopes, Instruments, and Systems **8**, 011024–011024 (2022)

35. B. Goncharov, L. Donnay, J. Harms, Inferring fundamental spacetime symmetries with gravitational-wave memory: from lisa to the einstein telescope. Phys. Rev. Lett. **132**, 241401 (2024)
36. S. Das, E.C. Vagenas, Phenomenological implications of the generalized uncertainty principle. Can. J. Phys. **87**, 233–240 (2009)
37. E. Sucu, İ. Sakallı, Y. Sucu, Multi-spin particle tunneling and black hole thermodynamics: Gup-corrected zitterbewegung and exponentially modified entropy, Physics Letters B, 140282 (2026)
38. G.G. Luciano, Y. Sekhmani, Generalized uncertainty principle mimicking dynamical dark energy: Matter perturbations and gravitational wave data analysis, arXiv preprint arXiv:2502.10043 (2025)
39. G. Gecim, Y. Sucu, Quantum gravity effect on the hawking radiation of spinning dilaton black hole. The European Physical Journal C **79**, 882 (2019)
40. E. Sucu, İ. Sakallı, Y. Sucu, Spin-dependent quantum corrections to Schwarzschild black hole thermodynamics with barrow entropy and GUP, https://doi.org/10.1142/s0219887826501161 (2026)
41. E. Sucu, I. Sakalli, Ads black holes in einstein-kalb-ramond gravity: Quantum corrections, phase transitions, and orbital dynamics, Nuclear Physics B **1018** (2025). https://doi.org/10.1016/j.nuclphysb.2025.117081
42. E.C. Vagenas, A. Farag Ali, and Hassan Alshal, Gup and the no-cloning theorem. The European Physical Journal C **79**, 276 (2019)
43. E. Sucu, I. Sakallı, Nonlinear electrodynamics effects on the geometry, thermodynamics, and quantum dynamics of (2+ 1)-dimensional black holes, Nuclear Physics B **116894** (2025)
44. G. Gecim, Y. Sucu, Quantum gravity correction to hawking radiation of the 2+ 1-dimensional wormhole. Adv. High Energy Phys. **2020**, 7516789 (2020)
45. E. Sucu, İ. Sakallı, Astrophysical reality of black hole thermodynamics and dynamics: Transformative influence of hernquist dark matter distributions, Physics of the Dark Universe , 102051 (2025)
46. G. Gecim, Y. Sucu, Quantum gravity effect on the tunneling particles from warped-ads3 black hole. Mod. Phys. Lett. A **33**, 1850164 (2018)
47. F. Ahmed, A. Al-Badawi, İ Sakallı, A. Bouzenada, Quasinormal modes and gup-corrected hawking radiation of btz black holes within modified gravity frameworks. Nucl. Phys. B **1011**, 116806 (2025)
48. G. Gecim, Y. Sucu, The gup effect on tunneling of massive vector bosons from the 2+ 1 dimensional black hole. Adv. High Energy Phys. **2018**, 7031767 (2018)
49. A. Al-Badawi, D.J. Gogoi, Y. Sekhmani, K. Boshkayev, Shadow and quasinormal modes of gup corrected grumiller black holes. Nucl. Phys. B **1015**, 116900 (2025)
50. İ Sakallı, Y. Sucu, E. Sucu, Zitterbewegung oscillations and GUP-induced quantum modifications of Yang-Mills black holes in perfect fluid dark matter. Nucl. Phys. B **1022**, 117216 (2026). https://doi.org/10.1016/j.nuclphysb.2025.117216
51. C. Tekincay, G. Gecim, Y. Sucu, Zitterbewegung particles tunneling from reissner-nordström ads black hole surrounded by quintessence. Europhys. Lett. **135**, 31003 (2021)
52. E. Sucu, Ä. Sakallı, Y. Sucu, Spin-dependent quantum corrections to schwarzschild black hole thermodynamics with barrow entropy and gup, International Journal of Geometric Methods in Modern Physics. **0**, 2650116 (0), https://doi.org/10.1142/S0219887826501161
53. C. Tekincay, M. Dernek, Y. Sucu, Exotic criticality of the btz black hole. The European Physical Journal Plus **136**, 222 (2021)
54. K. Nozari, B. Fazlpour, Generalized uncertainty principle, modified dispersion relations and the early universe thermodynamics. Gen. Relativ. Gravit. **38**, 1661–1679 (2006)
55. E. Sucu, I. Sakall, Quantum corrections and exotic criticality in charged rotating btz black holes, Physics of the Dark Universe, 102202 (2025)
56. N. Heidari, A.A.A. Filho, R.C. Pantig, A. Övgün, Absorption, scattering, geodesics, shadows and lensing phenomena of black holes in effective quantum gravity. Physics of the Dark Universe **47**, 101815 (2025)
57. C. Zhang, J. Lewandowski, Y. Ma, J. Yang, Black holes and covariance in effective quantum gravity. Phys. Rev. D **111**, L081504 (2025). https://doi.org/10.1103/PhysRevD.111.L081504. arXiv:2407.10168 [gr-qc]
58. A. Övgün, I. Sakallı, Hawking radiation via gauss-bonnet theorem. Ann. Phys. **413**, 168071 (2020)
59. S. Raju, Failure of the split property in gravity and the information paradox. Class. Quantum Gravity **39**, 064002 (2022)
60. P. Chen, Y.C. Ong, D. Yeom, Black Hole Remnants and the Information Loss Paradox. Phys. Rept. **603**, 1–45 (2015). https://doi.org/10.1016/j.physrep.2015.10.007. arXiv:1412.8366 [gr-qc]
61. R.J. Adler, P. Chen, D.I. Santiago, The Generalized uncertainty principle and black hole remnants. Gen. Rel. Grav. **33**, 2101–2108 (2001). https://doi.org/10.1023/A:1015281430411. arXiv:gr-qc/0106080
62. Y. Xiao, Y.-Y. Liu, First order corrections to black hole thermodynamics: A simple approach enhanced. Physical Review D **110**, 104043 (2024)
63. E. Sucu, İ Sakallı, Quantum-corrected thermodynamics and plasma lensing of mog black holes. Proceedings of the Royal Society A **481**, 20250251 (2025)
64. P. Jizba, G. Lambiase, Giuseppe Gaetano Luciano, and Luciano Petruzziello, Decoherence limit of quantum systems obeying generalized uncertainty principle: New paradigm for tsallis thermostatistics. Physical Review D **105**, L121501 (2022)
65. A. Alonso-Serrano, Mariusz P Dąbrowski, and Hussain Gohar, Nonextensive black hole entropy and quantum gravity effects at the last stages of evaporation. Physical Review D **103**, 026021 (2021)
66. S. Barman, G.M. Hossain, Consistent derivation of the Hawking effect for both nonextremal and extremal Kerr black holes. Phys. Rev. D **99**, 065010 (2019). https://doi.org/10.1103/PhysRevD.99.065010. arXiv:1809.09430 [gr-qc]
67. L. Vanzo, G. Acquaviva, R. Di Criscienzo, Tunnelling methods and Hawking's radiation: achievements and prospects. Class. Quant. Grav. **28**, 183001 (2011). https://doi.org/10.1088/0264-9381/28/18/183001. arXiv:1106.4153 [gr-qc]
68. H. Liu, M.-Y. Lai, X.-Y. Pan, H. Huang, D.-C. Zou, Gravitational lensing effect of black holes in effective quantum gravity. Physical Review D **110**, 104039 (2024)
69. Y. Lu, X.Y. Pan, M.Y. Lai, Q. Wang, Finite-distance gravitational lensing of a global monopole in schwarzschild-de sitter spacetime, arXiv preprint arXiv:2504.00777 (2025)
70. Z.-G. Guo et al., The Existence and Distribution of Photon Spheres Near Spherically Symmetric Black Holes - A Geometric Analysis. Eur. Phys. J. C **85**, 191 (2025). https://doi.org/10.1140/epjc/s10052-025-13872-2
71. G.W. Gibbons, The Jacobi-metric for timelike geodesics in static spacetimes. Class. Quant. Grav. **33**, 025004 (2016). https://doi.org/10.1088/0264-9381/33/2/025004. arXiv:1508.06755 [gr-qc]
72. S. Chanda, G.W. Gibbons, and Pv Guha, Jacobi-Maupertuis-Eisenhart metric and geodesic flows. J. Math. Phys. **58**, 032503 (2017). https://doi.org/10.1063/1.4978333. arXiv:1612.00375 [math-ph]
73. G. Crisnejo,E. Gallo, Weak lensing in a plasma medium and gravitational deflection of massive particles using the Gauss-Bonnet theorem. A unified treatment, Phys. Rev. D **97**, 124016 (2018) https://doi.org/10.1103/PhysRevD.97.124016arXiv:1804.05473 [gr-qc]
74. Z. Li, G. He, T. Zhou, Gravitational deflection of relativistic massive particles by wormholes, https://doi.org/10.1103/PhysRevD.101.044001 Phys. Rev. D **101**, 044001 (2020), arXiv:1908.01647 [gr-qc]

75. P. Das, Rv Sk, S. Ghosh, Motion of charged particle in Reissner–Nordström spacetime: a Jacobi-metric approach, https://doi.org/10.1140/epjc/s10052-017-5295-6 Eur. Phys. J. C **77**, 735 (2017), arXiv:1609.04577 [gr-qc]
76. G. W. Gibbons , M. C. Werner, Applications of the Gauss-Bonnet theorem to gravitational lensing, https://doi.org/10.1088/0264-9381/25/23/235009 Class. Quant. Grav. **25**, 235009 (2008), arXiv:0807.0854 [gr-qc]
77. Y. Huang, Z. Cao, Finite-distance gravitational deflection of massive particles by a rotating black hole in loop quantum gravity. The European Physical Journal C **83**, 80 (2023)
78. G. Crisnejo, E. Gallo, Weak lensing in a plasma medium and gravitational deflection of massive particles using the gauss-bonnet theorem. a unified treatment, Physical Review D **97**, 124016 (2018)
79. E. Sucu, İ Sakallı, Charged regular black holes in quantum gravity: from thermodynamic stability to observational phenomena. The European Physical Journal C **85**, 989 (2025)
80. G.S. Bisnovatyi-Kogan, O. Yu Tsupko, Gravitational lensing in a non-uniform plasma. Mon. Not. R. Astron. Soc. **404**, 1790–1800 (2010)
81. E. Sucu, İ. SakallÄś, Exploring lorentz-violating effects of kalb-ramond field on charged black hole thermodynamics and photon dynamics, Physical Review D **111**, 064049 (2025)
82. J. T. Mendonça, J. D. Rodrigues, H. Terças, Axion production in unstable magnetized plasmas, https://doi.org/10.1103/PhysRevD.101.051701 Phys. Rev. D **101**, 051701 (2020), arXiv:1901.05910 [physics.plasm-ph]
83. F. Wilczek, Two Applications of Axion Electrodynamics, https://doi.org/10.1103/PhysRevLett.58.1799 Phys. Rev. Lett. **58**, 1799 (1987)
84. J. L. Synge, ed., *Relativity: The General theory* (1960)
85. F. Atamurotov, K. Jusufi, Mv Jamil, A. Abdujabbarov, M. Azreg-Aïnou, Axion-plasmon or magnetized plasma effect on an observable shadow and gravitational lensing of a Schwarzschild black hole, https://doi.org/10.1103/PhysRevD.104.064053 Phys. Rev. D **104**, 064053 (2021), arXiv:2109.08150 [gr-qc]
86. C.A.O. Hare, Cosmology of axion dark matter, arXiv preprint arXiv:2403.17697 (2024)
87. A.O. Sushkov, Quantum science and the search for axion dark matter, PRX Quantum **4**, 020101 (2023)
88. S. Gillessen, F. Eisenhauer, S. Trippe, T. Alexander, R. Genzel, F. Martins, T. Ott, Monitoring stellar orbits around the massive black hole in the galactic center, The Astrophysical Journal **692**, 1075–1109 (2009)https://doi.org/10.1088/0004-637X/692/2/1075
89. S. Gillessen, P. M. Plewa, F. Eisenhauer, R. Sari, I. Waisberg, M. Habibi, O. Pfuhl, E. George, J. Dexter, S. von Fellenberg, T. Ott, R. Genzel, An update on monitoring stellar orbits in the galactic center, The Astrophysical Journal **837**, 30 (2017)https://doi.org/10.3847/1538-4357/aa5c41
90. G. Collaboration, R. Abuter, A. Amorim, M. Bauböck, J. P. Berger, H. Bonnet, *et al.*, Detection of the gravitational redshift in the orbit of the star s2 near the galactic centre massive black hole, Astronomy & Astrophysics **615**, L15 (2018) https://doi.org/10.1051/0004-6361/201833718
91. T. Do, A. Hees, A.M. Ghez, G.D. Martinez, D.S. Chu, S. Jia, S. Sakai, Jessica R. Lu, A. K. Gautam, K. K. O'Neil, et al., Relativistic redshift of the star s0-2 orbiting the galactic center supermassive black hole, Science **365**, 664–668 (2019)https://doi.org/10.1126/science.aav8137
92. A. Bera, S. Dalui, S. Ghosh, E.C. Vagenas, "Quantum corrections enhance chaos: Study of particle motion near a generalized Schwarzschild black hole" Phys. Lett. B **829** 137033 ,(2022) https://doi.org/10.1016/j.physletb.2022.137033arXiv:2109.00330 [gr-qc].